Geothermobarometry of the 2010 Eyjafjallajökull eruption: New constraints on Icelandic magma plumbing systems

J.K. Keiding, Olgeir Sigmarsson

Geothermobarometry of the 2010 Eyjafjallajökull eruption: New constraints on Icelandic magma plumbing systems

Jakob K. Keiding[1] and Olgeir Sigmarsson[2,3]

Received 31 August 2011; revised 29 November 2011; accepted 18 January 2012; published 14 March 2012.

[1] The 2010 Eyjafjallajökull eruption in Iceland produced mildly alkaline basalt that was emitted during the initial flank eruptive phase, whereas tephra predominately of benmorite composition was erupted during the second explosive phase from the summit of the volcano. These latter magmas show pervasive magma mingling between basalts and silicic magma. Glass and coexisting equilibrium mineral analyses have been used to define pressure-temperature crystallization paths for the eruption based on melt, clinopyroxene-melt and plagioclase-melt thermobarometry. Temperature calculations show that the early basaltic eruptions from the flank eruption have magmatic temperatures of around 1170°C (±25°C) and a narrow temperature range (<30°C) at any given depth. In contrast, benmoritic products crystallized at lower temperatures (1000–1060°C). Pressure estimates yield an average pressure of 5.6–6.4 kbar (±1.5 kbar) for the basaltic tephra and variable but lower pressures for the benmoritic samples ranging down to 0.6 kbar. The mafic magma mainly crystallized in the deeper crust (16–18 km), whereas mingled magma from the summit eruption crystallized at more shallow crustal levels (2–5 km) suggesting multistage magma ascent. Magmatic water concentrations were estimated with plagioclase-melt hygrometry. The maximum average water content of 1.8 wt % H_2O, obtained in one of the summit samples, is in agreement with melt inclusion observations. Water concentration of this or lower levels is demonstrated to only have limited effect on the pressure-temperature calculations.

Citation: Keiding, J. K., and O. Sigmarsson (2012), Geothermobarometry of the 2010 Eyjafjallajökull eruption: New constraints on Icelandic magma plumbing systems, *J. Geophys. Res.*, *117*, B00C09, doi:10.1029/2011JB008829.

1. Introduction

[2] The 2010 Eyjafjallajökull was characterized by very different magma composition and eruptive styles suggesting a complex magma plumbing system beneath the volcano. Key to improve understanding and models of magma plumbing systems, and how they evolve, is the knowledge of the depths at which magmas stagnate and partially crystallize. The pressure at which crystallization takes place is important to estimate because it influences the phase relationships and thereby the composition of the liquids [e.g., *O'Hara*, 1968; *Thy*, 1991]. Furthermore, the solubility of H_2O and other volatiles depend strongly on pressure [e.g., *Berndt et al.*, 2002; *Dixon et al.*, 1995; *Shishkina et al.*, 2010] that is of particular interest because exsolution of volatiles has a major impact on the eruption style and the physical dispersal of tephra. Assessment of magma emplacement depths is also needed to develop models for understanding and forecasting eruptions. In contrast to most other eruptions in Iceland during the last two decades, the Eyjafjallajökull volcano was not expected to erupt before the 2010 eruption although seismic unrest and inflation were monitored.

[3] Magma crystallization temperature is an intensive parameter of principal importance for characterization of magma chamber processes and the physical properties of volcanic eruptions. Thermal information is also critical for geophysical observations and models, as magma chamber temperatures affect variations in density and seismic velocity in the crust. Moreover, temperatures strongly control the viscosity of melts, which is one of the key parameters that determine for instance the transition between stable dome growth and potentially powerful explosions of silicic magma. Finally, quantification of the thermal budget during eruption is of particular interest at subglacial volcanoes like Eyjafjallajökull where insight to the melt-ice interaction, which possibly results in catastrophic jökulhlaups (meltwater floods), is critical for future hazard assessment in Iceland.

[4] Geodetic, seismological and gravimetrical methods have been applied to estimate pressure at magma emplacement or depths of magma chambers in Iceland [e.g., *de Zeeuw-van Dalfsen et al.*, 2006; *Key et al.*, 2011; *Pedersen and Sigmundsson*, 2004; *Sigmundsson et al.*, 2010; *Soosalu and Einarsson*, 2004; *Sturkell et al.*, 2003, 2006]. A different perspective on the question of emplacement depths may be gained from mineral-liquid pairs that

[1]GFZ German Research Centre for Geosciences, Potsdam, Germany.
[2]Laboratoire Magmas et Volcans, CNRS-Université Blaise Pascal, Clermont-Ferrand, France.
[3]Institute of Earth Sciences, University of Iceland, Iceland.

0148-0227/12/2011JB008829

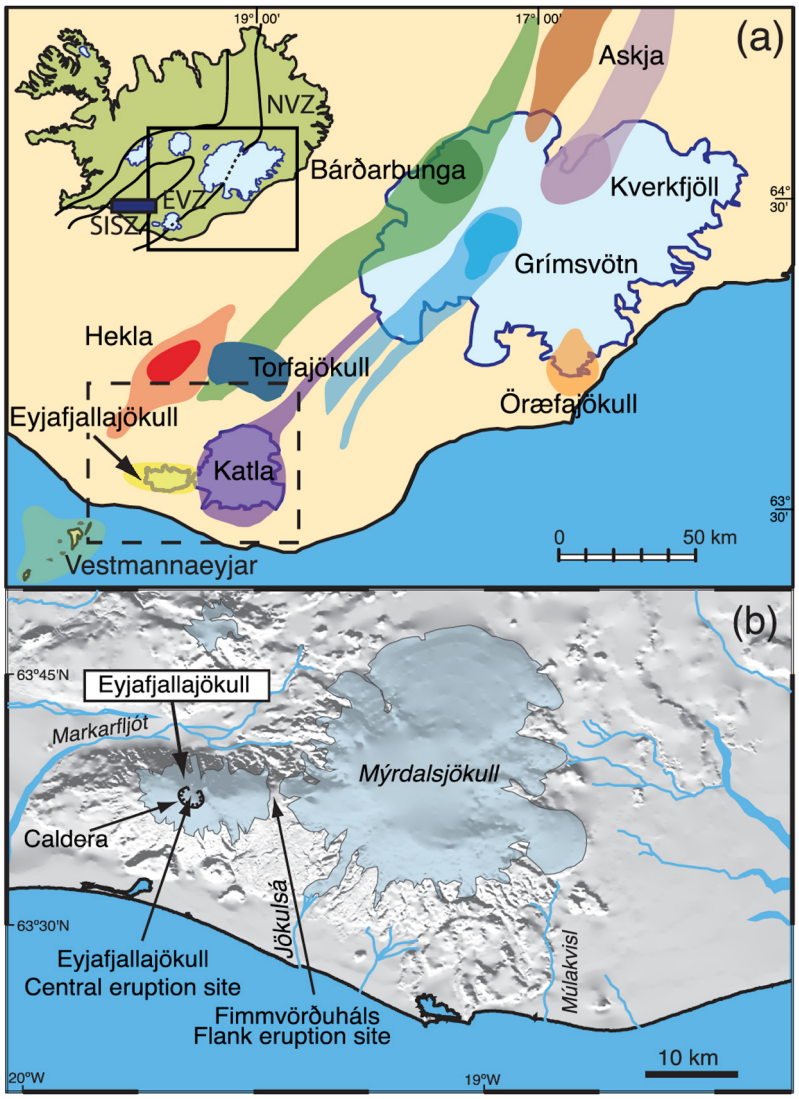

Figure 1. (a) Simplified geological map of SE Iceland showing location of the Eyjafjallajökull and other volcanic systems in the area. For clarity the small volcanic system Tindfjallajökull is not shown. Inset shows the neovolcanic zones of Iceland (EVZ: Eastern Volcanic Zone, NVZ: North Volcanic Zone; SISZ: South Iceland Seismic Zone). (b) Map of the Eyjafjallajökull area illustrating eruptions sites of the 2010 eruption. The eruption broke out at Fimmvörðuháls on 20 March. Starting on 14 April, eruptions took place at the summit caldera. Map modified from *Sturkell et al.* [2003].

provide an archive of the pressure conditions. *Klügel et al.* [2005] showed that pressure estimates based on petrological methods are better at resolving small magma batches that geophysical methods might not detect. In addition to constrain magma pressures such petrological methods also provide geothermometers and thus thermal information that is not directly available by other methods.

[5] Here, we examine mineral and coexisting melt compositions from tephra samples collected during the 2010 Eyjafjallajökull eruption. Our sample suite covers the temporal spectrum from the initial to the final phase of the eruption and thus provides a unique opportunity to study the net pressure-temperature evolution of the 2010 event. The geothermobarometry results are used to place constraints on magma storage depths and crystallization temperatures. Moreover, we test recently published hygrometers by *Putirka* [2008] and *Lange et al.* [2009] to quantify the H_2O content of the melts. Last, we compare our results to geophysical models on magma emplacement depths at the Eyjafjallajökull and previous estimates of crystallization temperatures in Iceland in general.

2. Geological Setting and Sampling

[6] The Eyjafjallajökull volcano (63° 38′ N, 19° 36′ W; 1666 m above sea level) in southern Iceland is an ice-covered stratovolcano characterized by quiescence compared to most other volcanoes in the Icelandic neovolcanic zone. It is located south of the rift-transform intersection where the Eastern Volcanic Zone (EVZ) and the South Iceland Seismic Zone (SISZ) meet (Figure 1). Prior to the 2010 eruption, the Eyjafjallajökull erupted in 1821 to 1823

and possibly in 1612 and around 920. Volcanic unrest, however, has been monitored more recently because of increased seismicity and inflation in 1994 and 1999 interpreted as emplacement of thin sill intrusions [*Pedersen and Sigmundsson*, 2004, 2006].

[7] The 2010 Eyjafjallajökull eruption broke out on 20 March after 3 months of precursory activity with a flank eruption at the Fimmvörðuháls Pass, between the Eyjafjallajökull and Mýrdalsjökull ice caps (Figure 1). This initial eruptive phase was manifested as two fissure eruptions on the north side of Fimmvörðuháls. The two fissures produced an aa lava flow field of plagioclase and olivine phyric basalt until 12 April. After a short cessation in eruptive activity the eruption moved to the west and broke out on 14 April beneath the Eyjafjallajökull summit crater or caldera (Figure 1). Due to the subglacial location the eruption was phreatomagmatic at the beginning, producing tephra that caused an unprecedented impact on aviation in large parts of Europe. The eruption changed from being phreatomagmatic to purely magmatic after less than a week and continued until 22 May.

[8] Tephra samples are used exclusively here for pressure-temperature calculations and consist of one sample from the Fimmvörðuháls flank eruption (FH-3) collected on 1 April from the opening phase of the second fissure. Three samples from the summit eruption were studied: EJ-2 that was produced 17–19 April, EJ-3 (collected freshly fallen on 22 April) and finally EJ-5 from 5 May.

3. Methods

3.1. Microprobe Data Acquisition

[9] Polished sections of tephra grains were prepared by standard procedures, embedding the tephra in epoxy, polishing and coating with carbon prior to in situ analyses. Major element concentrations of phenocrysts and glasses were analyzed on a SX-100 CAMECA electron microprobe (EMP) at Laboratoire Magmas et Volcans (Clermont-Ferrand, France) following the analytical setup described by *Sigmarsson et al.* [2011]. We used a 15 kV accelerating voltage, a 15 nA current, and a focused beam for the mineral analyses. For glasses, the electron beam current was lowered to 2–4 nA and a 10 μm defocused beam was employed to minimize sodium loss. All EMP analyses were carried out in manual mode after careful examination by backscattered electron (BSE) images prior to analysis (see below).

3.2. Thermobarometrical Calculations

[10] A large number of geothermometers and geobarometers have been developed for volcanic systems that can be summarized in three categories: (i) models based on chemical compositions of glasses or whole rock compositions (taken to be representative for liquid compositions) that are saturated with one or more crystal phases and how these liquids change with temperature and pressure [*Elthon*, 1989; *Herzberg*, 2004; *Lee et al.*, 2009; *Villiger et al.*, 2007; *Yang et al.*, 1996]; (ii) models dependent on crystal-chemical response to variations in pressure-temperature, which rely only on mineral compositions [*Lindsley*, 1983; *Nimis*, 1995; *Nimis and Ulmer*, 1998; *Powell and Powell*, 1974]; and finally, (iii) models using a combination of liquid and mineral equilibrium pairs which compositions are sensitive to pressures and/or temperatures [*Beattie*, 1993; *Kudo and Weill*, 1970; *Mathez*, 1973; *Putirka et al.*, 1996; *Putirka*, 2005, 2008; *Roeder and Emslie*, 1970]. Here we quantify temperature and pressure using the compositions of glasses, which unambiguously represent pre-eruptive liquid compositions, or glasses together with coexisting equilibrium mineral phases. This is preferable to methods that are solely based on mineral chemistry where features like mineral zoning, as observed in the present study, and the risk of xenocrystic origin of phenocrysts, as for instance invoked for anorthite-rich plagioclases in Iceland [*Halldorsson et al.*, 2008; *Hansen and Grönvold*, 2000; *Thorarinsson and Tegner*, 2009], can result in erroneous pressure-temperature estimates. Moreover, by working with glasses rather than whole-rock compositions we avoid the difficulties of correction for mineral accumulation that is particularly complicated when several minerals occur as phenocryst phases [*Mordick and Glazner*, 2006].

[11] Crystallization temperatures of plagioclase and clinopyroxene were calculated on the basis of *Putirka*'s [2008] equations 24a and 34, respectively. These two mineral-liquid thermometers were chosen because both plagioclase and clinopyroxene phases are common phenocrysts in all samples from the Eyjafjallajökull eruption and the models are calibrated for a large compositional range and have good precision (standard error of estimate [SEE] of $\pm 30^{\circ}$C for the applied thermometers [*Putirka*, 2008]).

[12] The pressure calculations are predominately based on the clinopyroxene-liquid barometer published by *Putirka* [2008] equation 30, which according to *Mollo et al.* [2010] gives the most accurate results of the different clinopyroxene-liquid geobarometers provided by *Putirka* [2008]. This model depends on the clinopyroxene jadeite-diopside-hedenbergite exchange between equilibrium liquid-clinopyroxene pairs combined with regression analyses of partial melting experiments with a standard error of ± 1.5 kbar [*Putirka*, 2008]. Pressure estimates were also carried out using the model of *Yang et al.* [1996] that depends solely on liquid compositions and pressure-dependent phase boundaries for melts saturated in plagioclase olivine and augite. The method is based on the principle that the composition of a melt in equilibrium with plagioclase, clinopyroxene and olivine is a function of pressure and works by predicting the phase boundaries for a given melt composition. This geobarometer or derivatives of it, based on phase relations in the pseudoternary planes in the system CaO–MgO–Al_2O_3–SiO_2 (CMAS) [*Elthon*, 1989], has been used widely on Icelandic basalts to determine crystallization pressures [*Breddam*, 2002; *Kelley and Barton*, 2008; *Maclennan et al.*, 2001; *Schiellerup*, 1995], but we limit the use of this approach to the flank eruption, as the model is only calibrated for basaltic liquids. Calculated pressures represent average pressure computed using the three equations by *Yang et al.* [1996] (i.e., projection from different minerals in the CMAS system) and has been performed through the downloadable Microsoft Excel spreadsheet available online as supplementary material to *Kelley and Barton* [2008].

[13] To this day no reliable geobarometer for olivine- or plagioclase-liquid pairs is available. *Finnerty and Boyd* [1978] showed that the Ca content of olivine in

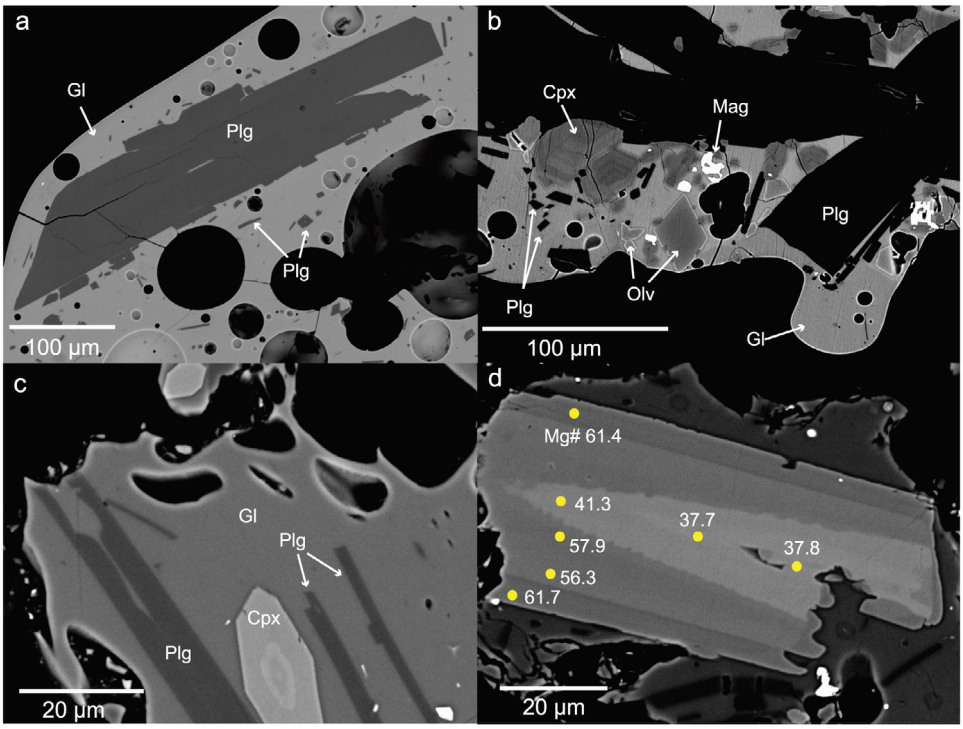

Figure 2. Backscattered electron images of tephra grains from the 2010 Eyjafjallajökull eruption. (a and b) High-MgO basalt emitted from the flank eruption at Fimmvörðuháls. Note the largely variable plagioclase crystal sizes, the zonation in clinopyroxene and thin Fe-rich (light-colored) rim compositions mantling the more Mg-rich olivine cores. Sample FH-3. (c) Benmorite tephra produced 17–19 April containing crystals of plagioclase and clinopyroxene. Sample EJ-2. (d) Close-up of reversely zoned clinopyroxene from benmoritic tephra erupted 5 May. Calculated Mg# from individual microprobe spot analyses is shown. Sample EJ-5. Abbreviations: Cpx, clinopyroxene; Gl, glass; Plg, plagioclase; Mag, magnetite; Olv, olivine.

equilibrium with pyroxene depends on pressure, however, the strong temperature sensitivity limits its use as a barometer and olivine is therefore only used as a geothermometer. Plagioclase shows some potential to constrain crystallization pressures as the mineral becomes more albitic with increasing pressure [*Panjasawatwong et al.*, 1995] and a geobarometer has been formulated by *Putirka* [2005], but results are ambiguous when comparing pressures obtained by this model to experimental data, and it is recommended only to use this geobarometer for natural compositions very similar to experimentally studied compositions where the model performs well [*Putirka*, 2008]. On the other hand, *Putirka* [2005] formulated a hygrometer that was basically a rearrangement of his thermometer allowing water concentration to be computed by fixing pressure and temperature from values obtained independently. We use a slightly modified version of this hygrometer published by *Putirka* [2008, equation 25b] that yields water contents to within ±1.1 wt % H_2O (SEE) for 730 hydrous experimental data [*Putirka*, 2008]. In addition, we also apply the hygrometer of *Lange et al.* [2009, equation 25] that are based on plagioclase-liquid exchange between the anorthite and albite components like other plagioclase hygrometers [*Housh and Luhr*, 1991; *Putirka*, 2005, 2008], but better incorporates calorimetric and volumetric dependencies on pressure and temperature and has a SEE of ±0.32 wt % H_2O. The plagioclase hygrometer calculations are based on temperatures obtained by the clinopyroxene thermometry rather than plagioclase temperatures to avoid circularity in using plagioclase to both obtain temperature and water content.

4. Results

4.1. Petrography, Mineral and Glass Geochemistry

[14] Here we will describe the petrography and summarize mineralogical and geochemical features of the Eyjafjallajökull eruptive products that are used for the geothermobarometry. More data from these samples are presented by *Sigmarsson et al.* [2011] and the reader is also referred to this paper for further interpretation of the geochemical data. Detailed work on the mineralogical variations will be presented elsewhere (O. Sigmarsson et al., manuscript in preparation).

[15] The basaltic tephra consists of highly vesicular lapilli size glass whereas the Eyjafjallajökull summit samples are characterized by a range of differently sized tephra grains from <10 μm to meter-sized bombs. In this study the size range of 50–250 μm was examined. Figure 2 shows typical tephra grains from the eruption used in the present study and illustrates the highly vesiculated nature of the magma. Olivine, plagioclase and clinopyroxene occur as phenocrysts with the two first phases often occurring together in glomerophyric aggregates. Minor and accessory minerals include chromium spinel (present as inclusions in olivine), magnetite, apatite, pyrite and orthopyroxene.

[16] Table 1 lists representative glass compositions, and all analyses can be found in Data Set S1 in the auxiliary

Table 1. Representative Electron Microprobe Analyses of Eyjafjallajökull Tephra[a]

Sample	Glass ID	SiO_2	TiO_2	Al_2O_3	FeO^T	MnO	MgO	CaO	Na_2O	K_2O	P_2O_5	Total	Mg#[b]
FH-3	FH-3/1	46.36	4.82	12.84	14.46	0.23	4.76	10.11	3.37	1.01	0.70	98.66	37
FH-3	FH-3/2	46.54	5.08	12.53	14.84	0.24	4.58	9.89	3.44	1.07	0.66	98.88	36
FH-3	FH-3/3	46.71	4.87	12.94	14.44	0.18	4.76	10.03	3.23	1.00	0.75	98.92	37
FH-3	FH-3/4	46.34	4.82	13.02	14.30	0.18	4.80	10.13	3.44	0.99	0.67	98.71	38
FH-3	FH-3/5	46.35	4.79	12.77	14.38	0.25	4.84	10.09	3.38	1.00	0.70	98.56	38
EJ-2	EJ-2/7	50.03	3.91	12.79	13.88	0.33	3.86	8.17	3.38	1.30	0.86	98.51	36
EJ-2	EJ-2/13	51.56	3.86	12.86	14.78	0.27	3.68	7.81	3.10	1.53	0.79	100.23	33
EJ-2	EJ-2/14	60.30	1.47	14.86	8.35	0.34	1.55	3.86	5.01	2.46	0.45	98.66	27
EJ-2	EJ-2/22	68.00	0.36	13.74	4.48	0.12	0.13	1.09	5.40	3.63	0.08	97.03	5.4
EJ-2	EJ-2/25	60.09	1.47	14.74	8.51	0.33	1.49	3.89	5.08	2.51	0.40	98.51	26
EJ-3	EJ3/5	58.24	2.09	14.77	9.26	0.26	1.96	4.80	4.90	2.26	0.44	99.00	30
EJ-3	EJ3/6	57.94	2.03	14.77	9.56	0.24	2.10	4.88	4.89	2.14	0.54	99.09	30
EJ-3	EJ3/9	57.45	2.01	14.77	9.75	0.23	2.16	4.85	4.95	2.22	0.54	98.93	31
EJ-3	EJ3/11	60.51	1.75	14.37	9.04	0.27	1.42	3.96	3.82	2.63	0.68	98.45	24
EJ-5	EJ-5/56	57.29	1.66	16.01	10.13	0.24	1.60	4.44	4.95	2.73	0.28	99.31	24
EJ-5	EJ-5/59	58.83	1.62	16.40	10.04	0.13	0.97	2.46	5.38	3.81	0.37	100.02	16
EJ-5	EJ-5 bis/12	61.76	1.49	14.45	8.20	0.14	1.37	3.28	4.30	2.88	0.44	98.30	25
EJ-5	EJ-5-II/15	63.76	1.36	14.33	8.17	0.24	1.44	3.19	2.56	2.94	0.65	98.63	26
EJ-5	EJ-5-II/26	64.27	0.71	14.29	7.32	0.38	0.83	2.00	5.46	3.27	0.29	98.82	18
EJ-5	EJ-5-II/28	66.13	0.49	14.86	5.55	0.32	0.53	1.92	5.67	3.54	0.20	99.22	16

[a]All oxides in wt %.
[b]Mg# = 100Mg/(Mg+Fe).

material.[1] Figure 3 is used for geochemical classification of the glasses analyzed and shows that they form an evolutionary trend that spans from alkali-rich basalt to mugearite to benmorite to trachyte to rhyolite. However, less alkaline glass compositions, are also observed particularly in sample EJ-5 where a considerable number of glass analyses plot below the alkaline-tholeiitic division line. The tephra glasses overlap with the bulk rock compositions reported by *Sigmarsson et al.* [2011], but the highly evolved compositions comparable to the 1821 Eyjafjallajökull rhyolite (Figure 3) are only recorded in the glass analyzed here and furthermore, the glass compositions display a continuum of compositions not observed in the bulk rock compositions. The large geochemical range observed in Eyjafjallajökull eruption was interpreted by *Sigmarsson et al.* [2011] as pervasive inhomogeneous magma mingling between basaltic and silicic end members of variable composition.

[17] Representative mineral chemical data for olivine, pyroxene and plagioclase phenocrysts are given in Table 2 and shown in Figure 4 all analyses can be found in Data Sets S2–S4. The olivine phenocrysts are euhedral and occasionally contain melt inclusions in addition to those of

[1]Auxiliary materials are available at ftp://ftp.agu.org/apend/jb/2011jb008829.

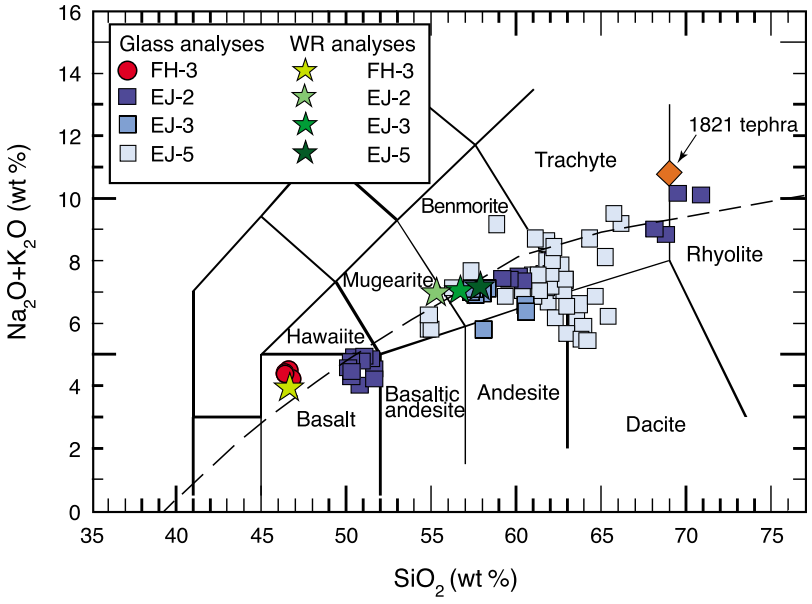

Figure 3. Total alkalies-silica (TAS) classification diagram after *Le Maitre et al.* [2005]. The alkaline-tholeiitic division line is from *Irvine and Baragar* [1971]. For comparison is also the 1821 Eyjafjallajökull rhyolite shown with a diamond symbol. Bulk rock compositions and 1821 Eyjafjallajökull rhyolite from *Sigmarsson et al.* [2011].

Table 2. Representative Compositions of Analyzed Eyjafjallajökull Minerals[a]

Sample	Label	SiO_2	TiO_2	Al_2O_3	FeO^T	MnO	MgO	CaO	Na_2O	K_2O	Total	Si	Ti	Al	Fe	Fe^{2+}	Fe^{3+}	Mn	Mg	Ca	Na	K	Sum	An	Ab	Or	En	Fs	Wo	Mg#	Fo
Olivine: Cations per 4 Oxygen Atoms																															
FH-3	FH-3/2	37.77	0.12	0.51	25.05	0.51	35.16	0.43			99.54	1.0015	0.002	0.016	0.555			0.011	1.390	0.012			2.988							71.4	
FH-3	FH-3/1	40.64	0.01	0.09	12.56	0.17	47.23	0.26			100.97	0.9985	0.000	0.003	0.258			0.004	1.730	0.007			3.000							87.0	
FH-3	FH-3/30	38.40	0.08	0.01	22.75	0.31	38.31	0.29			100.15	0.9997	0.002	0.000	0.495			0.007	1.487	0.008			2.999							75.0	
EJ-2	EJ-2/g1	36.76	0.25	0.33	30.98	0.51	30.26	0.68			99.78	1.0027	0.005	0.011	0.707			0.012	1.230	0.020			2.987							63.5	
EJ-2	EJ-2/24	41.07	0.84	2.79	27.37	0.52	25.70	1.87			100.20	0.9994	0.002	0.011	0.968			0.028	0.974	0.011			2.993							50.1	
EJ-3	EJ-3/g1	35.43	0.07	0.04	36.24	0.98	26.40	0.35			99.51	0.9988	0.002	0.001	0.854			0.023	1.109	0.011			2.999							56.5	
EJ-5	EJ-5/23	39.65	0.06	0.03	19.10	0.20	41.81	0.29			101.12	1.0025	0.001	0.001	0.404			0.004	1.576	0.008			2.996							79.6	
EJ-5	EJ-5-2/47	34.35	0.08	0.02	42.89	1.37	20.60	0.38			99.68	1.0030	0.002	0.001	1.047			0.034	0.897	0.012			2.995							46.1	
EJ-5	EJ-5 II/40	37.35	0.08	0.05	26.13	0.45	35.27	0.28			99.61	0.9958	0.002	0.002	0.583			0.010	1.402	0.008			3.002							70.6	
Pyroxene: Cations per 6 Oxygen Atoms																															
FH-3	FH-3/12	45.44	3.76	6.90	9.93	0.03	12.18	21.40	0.50	0.00	100.14	1.702	0.106	0.305		0.196	0.116	0.001	0.680	0.859	0.036	0.000	4.000				36.8	16.8	46.4		68.6
FH-3	FH-3/13	51.06	1.35	2.96	8.67	0.25	15.73	20.49	0.33	0.00	100.83	1.873	0.037	0.128		0.191	0.075	0.008	0.860	0.805	0.023	0.000	4.000				44.5	13.8	41.7		76.4
FH-3	FH-3/36	45.76	3.20	6.61	9.35	0.11	12.60	20.98	0.38	0.01	98.99	1.729	0.091	0.294		0.200	0.096	0.003	0.710	0.849	0.028	0.001	4.000				38.3	15.9	45.8		70.6
EJ-2	EJ-2/56	49.37	1.70	2.59	12.72	0.39	13.72	18.23	0.37	0.04	99.12	1.873	0.048	0.116		0.333	0.070	0.013	0.776	0.741	0.027	0.002	4.000				40.4	21.0	38.6		65.8
EJ-2	EJ-2/33	50.66	1.24	2.68	14.92	0.68	12.69	16.80	0.52	0.07	100.26	1.915	0.035	0.120		0.450	0.021	0.022	0.715	0.681	0.038	0.003	4.000				38.3	25.3	36.4		60.3
EJ-2	EJ-2/70	49.37	0.79	2.88	24.31	1.01	3.25	16.19	1.26	0.41	99.46	1.976	0.024	0.136		0.814	0.000	0.034	0.194	0.694	0.098	0.021	3.991				11.4	47.8	40.8		19.3
EJ-3	EJ-3/2	49.01	1.84	4.13	11.88	0.47	12.45	19.45	0.42	0.00	99.74	1.853	0.052	0.184		0.339	0.037	0.015	0.702	0.788	0.030	0.000	4.000				37.6	20.1	42.2		65.1
EJ-3	EJ-3/18	51.33	0.89	1.99	11.22	0.44	15.92	16.80	0.20	0.01	98.94	1.933	0.025	0.088		0.344	0.010	0.014	0.894	0.678	0.014	0.000	4.000				46.4	18.4	35.2		71.7
EJ-5	EJ-5/38	47.60	1.99	4.15	16.98	0.63	9.83	18.54	0.47	0.00	100.18	1.828	0.057	0.188		0.470	0.076	0.021	0.563	0.763	0.035	0.000	4.000				30.1	29.2	40.8		50.8
EJ-5	EJ-5bis/6	50.54	0.94	1.90	13.99	0.54	14.02	16.48	0.33	0.03	98.77	1.928	0.027	0.085		0.414	0.032	0.018	0.797	0.674	0.024	0.002	4.000				41.6	23.3	35.1		64.1
EJ-5	EJ-5bis/15	49.09	1.22	2.09	19.93	1.12	7.88	18.52	0.44	0.01	100.30	1.915	0.036	0.096		0.614	0.037	0.037	0.458	0.774	0.032	0.000	3.999				24.3	34.5	41.1		41.3
Feldspar: Cations per 8 Oxygen Atoms																															
FH-3	FH-3/32	52.17	0.14	29.46	0.70	0.17	0.14	13.06	3.63	0.17	99.64	2.385	0.005	1.587	0.027			0.003	0.010	0.640	0.322	0.010	4.988	65.8	33.1	1.0					
FH-3	FH-3/5	51.67	0.13	30.64	0.67	0.06	0.14	13.30	3.92	0.16	100.71	2.341	0.004	1.636	0.025			0.001	0.009	0.646	0.345	0.009	5.018	64.6	34.5	0.9					
FH-3	FH-3/21	50.61	0.11	30.72	0.94	0.00	0.13	13.77	3.47	0.14	99.89	2.316	0.004	1.657	0.036			0.000	0.009	0.675	0.308	0.008	5.013	68.1	31.1	0.8					
EJ-2	EJ-2/g1-1	55.30	0.20	28.15	0.98	0.00	0.16	10.74	5.26	0.30	101.09	2.480	0.007	1.488	0.037			0.000	0.011	0.516	0.458	0.017	5.013	52.1	46.2	1.7					
EJ-2	EJ-2/g15	64.94	0.03	20.55	0.64	0.05	0.04	1.25	8.91	3.45	99.88	2.902	0.001	1.082	0.024			0.001	0.003	0.060	0.772	0.197	5.041	5.8	75.1	19.1					
EJ-2	EJ-2/g11-2	59.43	0.14	25.44	0.81	0.03	0.08	7.21	7.01	0.43	100.59	2.648	0.005	1.336	0.030			0.001	0.005	0.344	0.606	0.024	4.999	35.3	62.2	2.5					
EJ-2	EJ-2 bis/64	69.26	0.05	18.47	0.81	0.01	0.01	0.19	7.74	5.00	101.54	3.031	0.002	0.953	0.030			0.000	0.001	0.009	0.656	0.279	4.960	1.0	69.5	29.6					
EJ-2	EJ-2 bis/65	66.83	0.09	18.91	1.23	0.01	0.00	0.27	8.97	3.38	99.69	2.981	0.003	0.994	0.046			0.000	0.000	0.013	0.775	0.192	5.006	1.3	79.1	19.6					
EJ-3	EJ-3/g1	58.35	0.11	26.12	0.79	0.04	0.09	8.21	6.56	0.40	100.68	2.605	0.004	1.374	0.030			0.001	0.006	0.393	0.568	0.023	5.003	39.9	57.7	2.3					
EJ-3	EJ-3/g2-1	58.52	0.17	26.49	0.80	0.04	0.05	8.24	6.47	0.43	101.20	2.599	0.006	1.387	0.030			0.001	0.003	0.392	0.557	0.025	4.998	40.3	57.2	2.5					
EJ-3	EJ-3/g2-2	61.08	0.13	24.80	0.78	0.00	0.06	6.24	7.39	0.72	101.19	2.698	0.004	1.291	0.029			0.000	0.004	0.295	0.633	0.040	4.994	30.5	65.3	4.2					
EJ-5	EJ-5/60	58.09	0.12	26.60	0.97	0.00	0.09	8.27	6.61	0.40	101.16	2.585	0.004	1.395	0.036			0.000	0.006	0.394	0.570	0.023	5.014	40.0	57.8	2.3					
EJ-5	EJ-5 bis/9	60.67	0.20	24.45	1.01	0.00	0.12	6.75	7.11	0.65	100.96	2.692	0.007	1.279	0.037			0.000	0.008	0.321	0.611	0.037	4.993	33.1	63.1	3.8					
EJ-5	EJ-5 bis/21	62.33	0.12	23.50	0.76	0.03	0.05	5.34	8.12	0.79	101.04	2.753	0.004	1.223	0.028			0.001	0.003	0.253	0.695	0.045	5.005	25.4	70.0	4.5					
EJ-5	EJ-5 bis/43	60.17	0.16	24.28	1.10	0.06	0.05	6.33	7.36	0.85	100.36	2.691	0.006	1.280	0.041			0.001	0.003	0.303	0.638	0.048	5.012	30.6	64.5	4.9					
EJ-5	EJ-5-5/30	65.07	0.02	21.00	0.34	0.05	0.00	2.63	9.32	1.12	99.53	2.890	0.001	1.099	0.013			0.001	0.000	0.125	0.802	0.063	4.994	12.6	81.0	6.4					

[a]All oxides in wt %. An = 100Ca/(Ca+Na+K), Ab = 100Na/(Ca+Na+K), Or = 100K/(Ca+Na+K), En = 100Mg/(Mg+Fe+Ca), Fs = 100Fe/(Mg+Fe+Ca), Wo = 100Ca/(Mg+Fe+Ca), Mg# (pyroxenes) and Fo (olivines) = 100Mg/(Mg+Fe). Fe^{2+}/Fe^{3+} ratio is estimated based on stoichiometric criteria as outlined by *Droop* [1987].

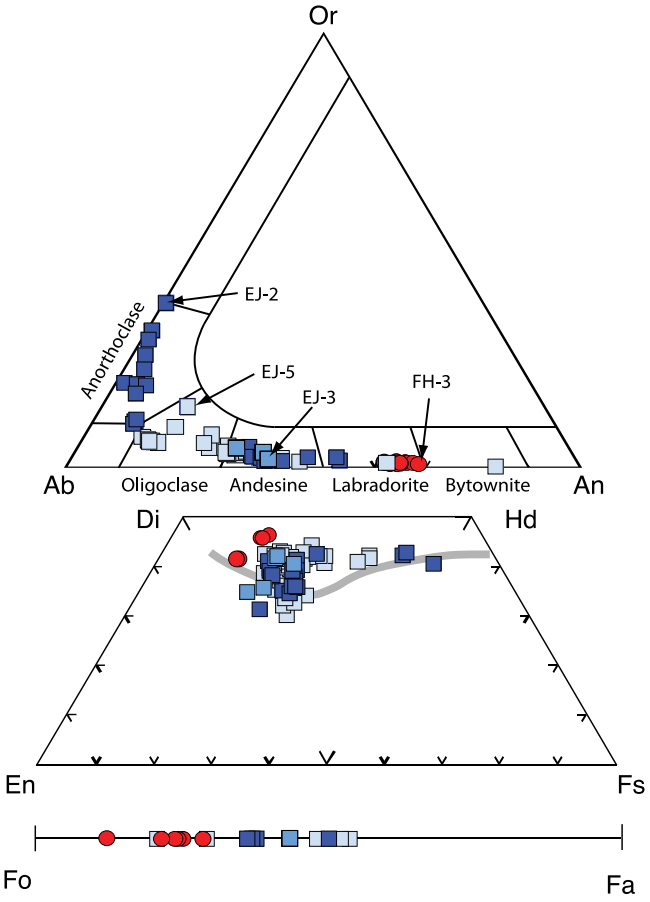

Figure 4. Summary of Eyjafjallajökull mineral composition illustrating the compositional evolution of phenocrysts. (top) Feldspar (An-Ab-Or), (middle) pyroxene (En-Di-Hd-Fs), and (bottom) olivine (Fo-Fa). For comparison the Skaergaard trend from *Wager and Brown* [1968] is shown as a gray curve in the pyroxene trapezoid.

chromium spinel. Olivines span the compositional range $Fo_{87.0–46.1}$ with the most magnesian olivines found in sample FH-3 from the flank eruption. But primitive olivine compositions are also found in the cores of EJ-5 from the summit eruption indicating magma mingling. The olivines are often normally zoned sometimes with only thin (5–10 μm) rims of Fe-rich olivines that mantle more Mg-rich cores (Figure 2b).

[18] Clinopyroxenes are euhedral to subhedral and predominantly lath shaped to tabular. Their compositions show significant variations ($Wo_{31–46}En_{11–56}Fs_{14–48}$) and classify as augites in the quadrilateral plot [*Morimoto*, 1989]. The compositional variability is also illustrated in clinopyroxene Mg# (molar Mg over Mg and Fe) that varies between 76 and 19 (Table 2 and Data Set S4) with the most primitive compositions observed in the basaltic sample. In comparison the three samples from the summit eruption have as expected generally more evolved compositions but also show larger intersample variability in their mineral chemistry. Zoning is common in the clinopyroxenes and is frequently reversed (Figure 2d) with variations in $\Delta Mg\# \leq 25$ between core and rim. Na_2O concentrations typically range between 0.20 and 0.73 wt % generally negatively correlated with the Mg#.

[19] Feldspar crystals occur both as phenocrysts and groundmass phase and are characterized by euhedral to subhedral crystals with prismatic to equant morphologies. The analyses of feldspars are plotted in the ternary classification diagram albite-anorthite-orthoclase (Figure 4) and illustrate how they evolve from anorthite-rich plagioclase to alkali feldspar. Plagioclase composition from the flank eruption defines a relative restricted range of $An_{68.1–61.3}$ compare to the more evolved plagioclases from the summit samples dominated by oligoclase to andesine compositions. Both normal and reversed zonation is common in the plagioclases. Sample EJ-5 contains the most primitive plagioclase measured ($An_{83.3}$) interpreted as being of xenocrystic origin. Anorthoclase is only observed in sample EJ-2 found in microgranite fragments that also contain the most Fe-rich augites [see *Sigmarsson et al.*, 2011].

4.2. Test of Mineral-Melt Equilibrium

[20] An important prerequisite to use the applied thermobarometers is to test that mineral and liquid represent coexisting equilibrium pairs. This procedure is necessary to avoid crystal–whole-rock pairs unlikely to yield valid pressure-temperature estimates. As a first step visual information was used qualitatively to ensure that texturally there was evidence for equilibration of the minerals and crystals. Thus as a standard analytical procedure, grains that morphologically reflect disequilibrium with unreacted parts or patchy zoning, judging from the mean atomic density BSE images, were avoided. In general, the predominant euhedral nature of the crystals (Figure 2) indicates that the crystals are in equilibrium with the surrounding liquid. On the other hand, however, the strongly zoned nature of the phenocrysts described above implies that the minerals crystallized from liquids of different compositions. Here we use crystal rims for the geothermobarometry calculations if the margins are in equilibrium with the surrounding liquid even if the cores of the crystals are not.

[21] Mineral-liquid equilibrium was also examined by comparing Mg-Fe and albite-anorthite partitioning between liquid and clinopyroxene and liquid and plagioclase, respectively. The exchange coefficient of Fe-Mg between clinopyroxene and liquid ($K_D^{cpx–liq}$ (Fe-Mg) = $[MgO^{liq}FeO^{cpx}]/[MgO^{cpx}FeO^{liq}]$ where MgO and FeO are molar fractions) are frequently used to test equilibrium between clinopyroxene and liquid [e.g., *Aulinas et al.*, 2010; *Maclennan et al.*, 2001; *Stroncik et al.*, 2009]. Here, we accept samples that fall within a range of 0.28 ± 0.08 [*Putirka*, 2008]. Figure 5a shows the relationship between Mg/(Mg+Fe) of clinopyroxenes and coexisting glass compositions and illustrates that Mg numbers of the clinopyroxenes agree in most cases with those predicted from the glass analyses. However, for the sample EJ-5 a considerable number of clinopyroxenes plot to the left of the equilibrium lines indicating a nonequilibrium nature of these crystals. For plagioclase we test equilibrium by the anorthite-albite exchange coefficient ($K_D^{plg/liq}$ (An-Ab) = $[Ab^{plg}Al_2O_3^{liq}]/[An^{plg}Na_2O^{liq}SiO_2^{liq}]$ where all components are in molar fractions) using $K_D^{plg/liq}$ (An-Ab) = 0.27 ± 0.11 [*Putirka*, 2008]. The histogram in Figure 5b of plagioclase $K_D^{plg/liq}$ (An-Ab) shows dominant frequency within the accepted values. Mineral-liquid pairs outside the accepted exchange coefficient values for clinopyroxene and plagioclase were discarded for further geothermobarometry analyses.

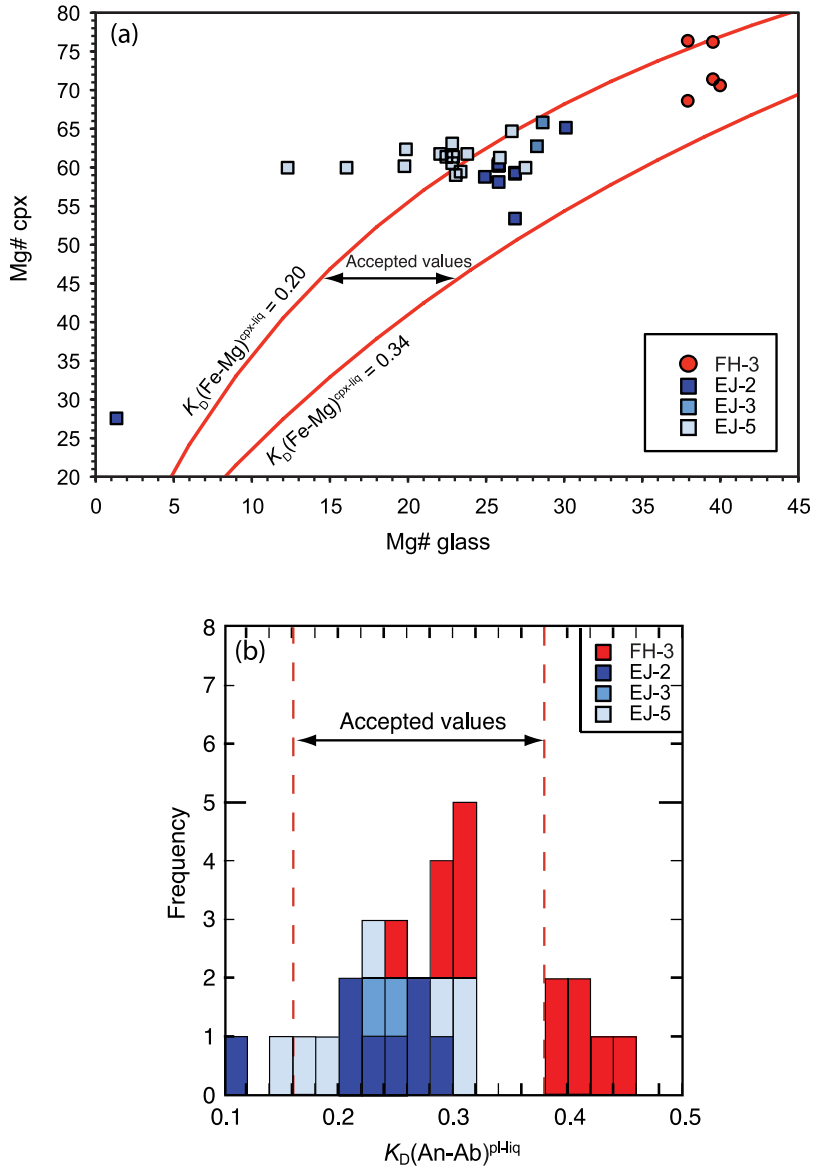

Figure 5. Test of equilibrium between phenocrysts and glass compositions. (a) MgO-FeO relationship between glass and coexisting clinopyroxenes. The equilibrium constant K_D (red lines) describes Mg-Fe partitioning between crystals and liquid. Note that many pyroxenes are more Fe-rich than the host rock in which they occur. (b) Frequency histogram for plagioclase showing the distribution of equilibrium constant K_D based on albite-anorthite component distribution between plagioclase and coexisting liquid (see text for further description). The accepted range of equilibrium constant values for both Figures 5a and 5b is from *Putirka* [2008].

4.3. Thermobarometry Results

[22] Results of geothermometric calculations are presented in Table 3 and Figures 6–7. After applying the mineral-liquid equilibrium filters, plagioclase thermometry shows that the early basaltic eruptions at Fimmvörðuháls have magmatic (anhydrous) temperatures of ~1170°C and a narrow temperature range (~15°C). In contrast, benmorites crystallized at lower temperatures (1010–1063°C) deduced from the most primitive feldspar compositions used here. The clinopyroxene thermometer gives results between 981°C and 1193°C (Table 3) generally showing slightly lower temperatures (10–15°C) than plagioclase-liquid data for the summit eruption but in good agreement with these data as illustrated in Figure 6.

[23] Pressure estimates based on the clinopyroxene-liquid pairs (on an anhydrous basis) yield 4.5–7.1 kbar and −1.2–4.2 kbar for the flank eruption and the summit eruption, respectively (Table 3), and show generally positive correlation with the clinopyroxene Mg# (Figure 7). The summit eruption is characterized by larger scatter in the calculated pressures ranging down to very shallow pressures and giving slightly negative pressures for some of the crystal-liquid pairs from sample EJ-2 and EJ-5 (Figure 7). Computed mean

Table 3. Geothermobarometry and Hygrometry Results

	Liquid				Clinopyroxene-Liquid				Plagioclase-Liquid					
Sample	Glass ID	Mg#[a]	P (kbar) Equations 1–3[b]	Cpx ID	Cpx Mg#[a]	K_D(Fe-Mg)	P (kbar) Equation 30[c]	T (°C) Equation 34[c]	Plag ID	An[a]	K_D(Ab-An)	T (°C) Equation 24a[c]	H_2O (wt %) Equation 25b[c]	H_2O (wt %) Equation 25[c]
FH-3	FH-3/1	37.0	6.5	FH-3/12	68.6	0.25	4.5	1161	FH-3/6	63.9	0.29	1169	−1.8	0.9
FH-3	FH-3/2	35.5	6.5	FH-3/23	71.4	0.24	7.1	1193	FH-3/34	67.0	0.30	1168	−2.3	0.5
FH-3	FH-3/3	37.0	6.0	FH-3/22	76.2	0.20	5.6	1173	FH-3/14	61.3	0.31	1161	−1.9	0.6
FH-3	FH-3/4	37.5	6.5	FH-3/36	70.6	0.25	5.2	1175	FH-3/21	68.1	0.26	1174	−1.8	0.9
FH-3	FH-3/5	37.5	6.4						FH-3/24	62.6	0.31	1168	−1.8	0.7
FH-3									FH-3/35	64.4	0.29	1168	−1.8	0.8
FH-3 average		37.2	6.4		71.7	0.24	5.6	1175		64.7	0.29	1168	−1.9	0.7
FH-3 S.D.[d]		0.8	0.2		1.4	0.01	1.4	16		2.5	0.02	4	0.2	0.1
EJ-2				EJ-2/46	59.3	0.23	3.0	1054	EJ-2/g5	36.3	0.21	1052	1.5	1.5
EJ-2				EJ-2/47	53.4	0.29	1.1	1043	EJ-2/g4	45.6	0.23	1054	1.7	1.4
EJ-2				EJ-2/48	59.2	0.23	−0.2	1032	EJ-2/g9-2	32.8	0.24	1059	1.6	1.4
EJ-2				EJ-2/26	60.2	0.21	−0.6	1025	EJ-2/g11-1	29.2	0.28	1043	2.6	1.1
EJ-2				EJ-2/27	60.4	0.20	1.6	1041	EJ-2/g11-2	35.3	0.22	1050	1.5	1.4
EJ-2				EJ-2/33	60.3	0.21	2.7	1047	EJ-2/g11-3	32.9	0.24	1050	1.7	1.2
EJ-2				EJ-2/32	58.1	0.23	4.2	1056	EJ-2/g9-1	31.0	0.27	1054	1.9	1.3
EJ-2 average					58.7	0.23	1.7	1043		33.9	0.24	1051	1.8	1.3
EJ-2 S.D.[d]					2.5	0.03	1.8	11		4.7	0.03	4	0.4	0.2
EJ-3				EJ-3/2	65.1	0.21	2.1	1063	EJ-3/g1	39.9	0.23	1061	1.3	1.2
EJ-3				EJ-3/16	65.8	0.20	1.5	1060	EJ-3/g2-1	40.3	0.24	1063	1.4	1.4
EJ-3 average					65.5	0.20	1.8	1062		39.9	0.24	1061	1.4	1.3
EJ-3 S.D.[d]					0.5	0.01	0.4	2		0	0.01	2	0.1	0.2
EJ-5									EJ-5/31	26.4	0.31	1010	2.6	0.9
EJ-5				EJ-5/50	59.4	0.20	0.8	981	EJ-5/57	31.3	0.22	1056	1.2	1.7
EJ-5				EJ-5-II/12	50.7	0.23	−1.2	1008	EJ-5-5/1	37.9	0.29	1055	1.5	0.7
EJ-5				EJ-5-II/10	59.0	0.19	0.2	1029	EJ-5/64	37.5	0.31	1029	1.2	1.1
EJ-5				EJ-5-II/14	61.2	0.20	2.7	1004	EJ-5ol/13	40.5	0.16	1038	1.2	2.2
EJ-5									EJ-5 bis/11	36.8	0.19	1034	2.1	1.8
EJ-5 average					57.6	0.20	0.6	1006		36.8	0.27	1040	1.6	1.4
EJ-5 S.D.[d]					4.7	0.02	1.6	20		3.9	0.05	26	0.6	0.6

[a]Cpx Mg# and Mg# (of glass) = 100Mg/(Mg+Fe). An = 100Ca/(Ca+Na+K).
[b]Equations 1–3 from *Yang et al.* [1996].
[c]Equation 25 from *Lange et al.* [2009]. Other equations from *Putirka* [2008].
[d]S.D. is standard deviation (one sigma).

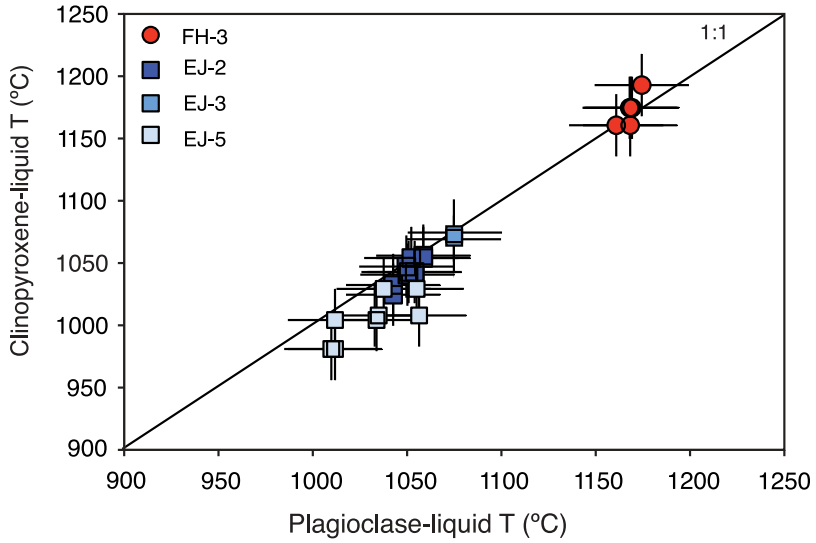

Figure 6. Calculated crystallization temperatures for clinopyroxene-liquid versus plagioclase-liquid pairs. Error bars show the SEE of the geothermometer methods [*Putirka*, 2008].

pressures range from 5.6 kbar for the basaltic tephra to 0.6–1.8 kbar for the benmorites from the summit eruption liquid. Using the model of *Yang et al.* [1996] gives pressures of 6.0–6.5 kbar for the basaltic flank eruption (Table 3) with an average of 6.4 kbar, which is within error of the results obtained from the clinopyroxene-liquid geobarometer.

4.4. H_2O Estimates

[24] The water concentrations obtained using the two plagioclase hygrometers are listed in Table 3. Employing the *Putirka* [2008] model on the basaltic FH-3 sample gives negative concentrations of −1.8 wt % to −2.3 wt % H_2O interpreted as anhydrous melt compositions. Calculated water concentrations using this hygrometer for the summit eruption are in the range 1.2–2.6 wt % water with average composition of 1.4 wt % H_2O to 1.8 wt % H_2O in the three EJ samples with the highest water concentration observed in sample EJ-2. Application of the *Lange et al.* [2009] model gives 0.5–0.9 wt % H_2O for the basaltic flank eruption and 0.7–2.2 wt % H_2O for the benmoritic summit eruption, with average water concentrations for the summit samples in a narrow range of 1.3–1.4 wt % H_2O.

5. Discussion

5.1. Effect of H_2O on Pressure-Temperature Estimates

[25] The pressure-temperature calculations at this point is based on nominally anhydrous conditions, however, our hygrometry calculations indicate that H_2O is a significant component at least for the evolved tephra as also confirmed

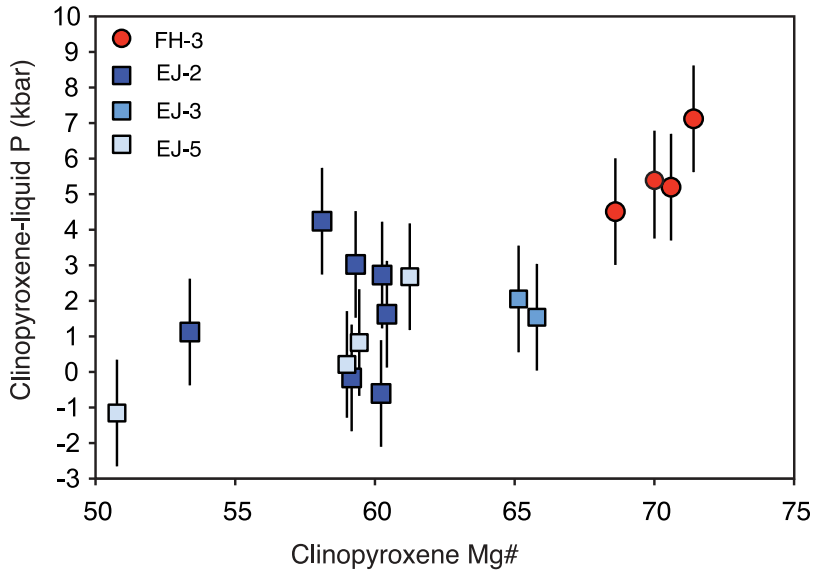

Figure 7. Pressure estimates based on clinopyroxene-liquid barometry versus Mg# of clinopyroxenes. Error bars show the SEE of the applied geobarometer method [*Putirka*, 2008].

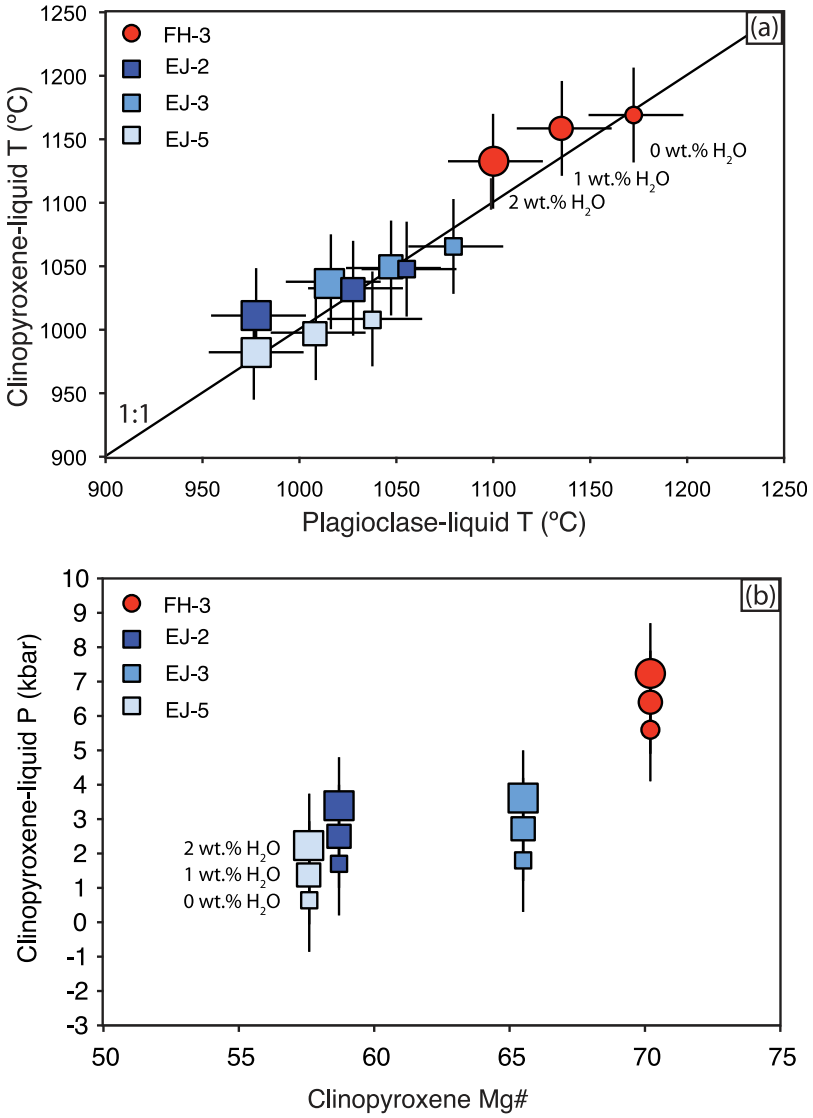

Figure 8. Effect of H_2O on temperature and pressure estimates. (a) Mean clinopyroxene-liquid temperatures versus mean plagioclase-liquid temperatures. (b) Average pressures for clinopyroxene-liquid barometry versus mean clinopyroxene Mg# for each of the studied samples. Increasing size of symbols denote higher water content in the melt. Small symbols = 0 wt % H_2O, medium symbols = 1 wt % H_2O, and large symbols = 2 wt % H_2O. Error bars show the SEE of the applied geothermobarometry methods [*Putirka*, 2008].

by melt inclusions studies (see discussion below). Thus it is important to evaluate the effect of water on our intensive parameter calculations. Figure 8a illustrates the impact on crystallization temperature for the two geothermometer adding one and two percent H_2O, which is considered to be the maximum concentration of water dissolved into the flank and summit liquids, respectively. As expected the calculated crystallization temperatures are shifted to lower values when water is added as a component. The temperature decrease is relative minor but most important for plagioclase crystallization temperatures, diminishing by 30–40°C from 1 wt % H_2O addition in comparison to clinopyroxene temperatures, which are lowered by 10–15°C. Also the clinopyroxene barometer used here is dependent on the water content of the liquid as illustrated in Figure 8b. Adding 2 wt % H_2O increases the pressure by 1.6 kbar, which is about the uncertainty of the clinopyroxene-liquid geobarometer (±1.5 kbar). The pressure calculations based on work by *Yang et al.* [1996] would also be affected by the water concentration of the liquid, as the stability field of plagioclase is enlarged at the expense of the olivine stability field under hydrous conditions [*Kushiro*, 1969; *Sisson and Grove*, 1993]. Unfortunately, it is not possible to quantify the effect water has on these pressure calculations as the model by *Yang et al.* [1996] is based on a nominal water free basis and the effect of water is not incorporated into the model. We concur with *Kelley and Barton* [2008] who argued that pressure calculations based on the predicted position of the olivine-augite-plagioclase-melt saturation boundaries would only be slightly affected by basaltic liquids with 0–1 wt % H_2O. In summary, we conclude that our temperature and pressure calculations show only limited dependency of the water content of the melt.

5.2. Emplacement Model and the Plumbing System

[26] The density of the Icelandic crust shows a large range between 1800 kg/m^3 for unconsolidated hyaloclastite to about 3000 kg/m^3 for the deep crust [*Gudmundsson*, 2003; *Menke*, 1999; *Schopka et al.*, 2006]. Here we use a weighted mean value of 2800 kg/m^3 to convert our pressure estimates to depths. We suggest that primitive basalt of deep origin was injected into the plumbing system of the Eyjafjallajökull volcano during the period December 2009 to 20 March 2010 as indicated by the continuous seismic and GPS monitoring stations [*Gudmundsson et al.*, 2010; *Sigmundsson et al.*, 2010]. This liquid partially crystallized in a deep-seated magma chamber at a depth of 16–18 km. After 3 months halt in migration of the magma, eruption of primitive basalt magma (1160–1170°C) broke out as a flank eruption. Three weeks later, the older and partially crystallized basalt remobilized and mingled with a rhyolitic magma body at shallower depth of 2–5 km directly beneath the summit crater as observed in the more evolved chemical compositions (Figure 2) and lower pressure estimates of the late-stage volcanic products. We envisage that the summit samples crystallized at decreasing depth with time as also supported by lower average pressure obtained in sample EJ-5 compared to EJ-2 (Table 3), however, the precision of the clinopyroxene geobarometer and the scatter in the data unfortunately cannot preclude that all the summit samples essential crystallized at the same pressure. A detailed study based on fluid inclusion densities could possible resolve this issue.

5.3. Comparison to Other Studies

[27] To test our hygrometry calculations, we compare the results to analyses of melt inclusions. These are contained in relatively incompressible crystals and the melt inclusions will ideally retain the volatile contents of the undegassed magmas [*Kent*, 2008; *Lowenstern*, 1995; *Roedder*, 1984]. *Moune et al.* [2012] analyzed a limited number of olivine-hosted melt inclusions by ion microprobe from the basaltic flank eruption and obtained H_2O concentrations of 0.82–0.95 wt % and *Thordarson et al.* [2011] found 1.7 wt % water in plagioclase-hosted melt inclusions from the benmoritic summit eruption. The hygrometer of *Putirka* [2008] predicting average 1.3–1.8 wt % for the three summit samples is in excellent agreement with the melt inclusion data, whereas the basaltic samples clearly underestimate the water concentrations. Based on our limited data set, we speculate that the hygrometer is better calibrated for fairly evolved hydrous samples than basaltic liquids. The model of *Lange et al.* [2009] predicts the H_2O concentrations in the basalts better (average 0.7 wt % H_2O) with similar water concentrations in the evolved samples (average 1.3–1.4 wt % H_2O). Still, this model performs reasonable well considering the associated errors of our temperature estimates. Furthermore, we apply the hygrometer to plagioclases that in some instances are slightly outside the range that this model is calibrated for (An_{37}-An_{93}). We find that the hygrometer of *Lange et al.* [2009] is better at predicting water concentrations in Eyjafjallajökull than the Putirka model, whereas *Mollo et al.* [2011] came to the opposite conclusion in their study of basalts from Etna. Further studies are thus needed for quantitative comparison of the two plagioclase hygrometers before precise estimations of water concentrations in igneous rocks.

[28] To the best of our knowledge this is the first attempt to estimate crystallization temperatures from the Eyjafjallajökull volcanic system. Thus no direct comparison to previous thermometry is possible, but our maximum average temperature of 1175°C for the basaltic flank eruption agree well with those reported by *Kelley and Barton* [2008] for basalts erupted from more than 30 volcanic centers covering all major rifting zones in Iceland and is similar to that measured during the emission of mildly alkali basalts at Surtsey Island by T. Sigurgeisson [*Sigmarsson et al.*, 2009, and references therein]. Moreover, this estimate lies in the middle of the range of temperatures for Icelandic basalts from ~1130°C as the minimum crystallization temperatures for the Iceland Fe-Ti basalts [*Óladóttir et al.*, 2008, and references therein] to 1240°C for picrites and primitive ol-tholeiites [*Breddam*, 2002; *Schiellerup*, 1995] and 60–70°C lower than estimates from homogenization runs of olivine and plagioclase hosted melt inclusions [*Gurenko and Chaussidon*, 1995; *Hansen and Grönvold*, 2000; *Hansteen*, 1991]. The crystallization temperatures for the summit eruption (1000–1060°C) are comparable to the highest estimated temperatures of icelandite and Icelandic rhyolites [e.g., *Sigurdsson and Sparks*, 1981] and to the fluid-absent melting temperatures of amphibolites yielding evolved dacite composition close to those of Hekla volcano [*Sigmarsson et al.*, 1992].

[29] Contrary to crystallization temperatures, magma emplacement depths beneath the Eyjafjallajökull volcanic system have been estimated in several studies. *Sturkell et al.* [2003] observed deformation by tiltmeters and GPS measurements after the 1999 volcanic unrest. They explained the deformation by magma emplacement beneath the southern flank of the volcano modeled from a point pressure source at 3.5 km depth. Another approach was taken by *Pedersen and Sigmundsson* [2004, 2006] who used models based on interferometric satellite radar (InSAR) and seismic data to monitor inflation in the volcano. Their models suggest the deformation source at a depth of 6.3 km depth interpreted as thin sills intruded in the upper crust. Most recently, *Sigmundsson et al.* [2010] through joint inversion of GPS and InSAR data modeled the depth of magma emplacement for the 2010 eruption as a two-phase sill inflation. The first phase was derived from depths of 4.0–5.9 km whereas the second sill was emplaced at about the same depth under the northeastern flank of the volcano, together with a southeast tilted dyke reaching from 3.2 to 6.1 km depth. Our depth estimates for the benmoritic eruption (1.7–5.0 km) compare well with the deformation modeling results. In contrast, the deep-seated magma reservoir proposed here for the Fimmvörðuháls flank eruption deviates from all previous pressure estimates of the Eyjafjallajökull volcanic system. As summarized by *Kelley and Barton* [2008], however, there is substantial geophysical and petrological evidence for magma chambers in the middle and lower crust (depths >7 km) in Iceland [see also *Breddam*, 2002; *Furman et al.*, 1991; *Key et al.*, 2011; *Slater et al.*, 2001; *Soosalu and Einarsson*, 2004; *Soosalu et al.*, 2010; *Thy*, 1991; *White et al.*, 2011]. These deep-seated magma chambers have been inferred to aliment eruptions generating the large shield volcanoes in late Pleistocene/early Holocene time [e.g., *de Zeeuw-van*

Dalfsen et al., 2004; *Maclennan et al.*, 2001; *Slater et al.*, 2001] but have also been proposed by *Hards et al.* [2000] to reflect the tectonic setting with deep empheral alkaline magma chambers generated at the tip of the propagating rift zone inferred beneath the Vestmannaeyjar archipelago (Figure 1a) [*Furman et al.*, 1991; *Thy*, 1991] whereas tholeiites are formed in mature rift zones at shallower depth often fed by frequent magma replenishment.

[30] Interestingly, modeling of the magma chamber depth of the volcano Katla, located just 25 km east of Eyjafjallajökull (Figure 1), based on geophysical observations results in relatively shallow magma chambers (1–5 km) [*Gudmundsson et al.*, 1994; *Soosalu et al.*, 2006; *Sturkell et al.*, 2003], whereas *Kelley and Barton* [2008] using the *Yang et al.* [1996] methods, also employed in this study, calculated depths in excess of 15 km for basaltic Katla glasses. This mismatch could indicate magma reservoirs at different depths beneath Katla. Indeed, *Óladóttir et al.* [2008] observed a wide range of composition for Katla magmas during the Holocene and proposed a complex plumbing system where temporal variations in K_2O concentrations in tephra reflect changes in the depth and magma chamber configuration from where magma is extracted. Although Eyjafjallajökull and Katla volcanoes are different in terms of size it is likely that they have magma plumbing systems that evolve comparably with time due to their similar tectonic setting.

[31] Multiple magma chambers at different depths beneath single volcanoes are not unique to Katla or Eyjafjallajökull but have been proposed in several volcanic systems [e.g., *Schiellerup*, 1995; *de Zeeuw-van Dalfsen et al.*, 2004, 2006; *Sturkell et al.*, 2006]. Our results reinforce the conclusion that magma reservoirs are common in both the lower and shallower crust in Iceland.

6. Summary and Conclusions

[32] (1) The 2010 Eyjafjallajökull eruption records the evolution from fairly primitive basalt erupted at the flank eruption to highly differentiated tephra dominated by benmoritic compositions emitted from the explosive summit eruption. Reverse mineral zonation, and highly variable mineral and glass compositions indicate magma mingling and mixing in a complex magmatic plumbing system beneath the Eyjafjallajökull volcano tapping melt from different sources.

[33] (2) Clinopyroxene-liquid and plagioclase-liquid geothermometry are correlated and show that the basaltic tephra from the flank eruption crystallized at 1170°C and the benmorite tephra samples crystallized from 1000°C to 1060°C. These thermometry results compare well with previously published estimates from Icelandic volcanoes.

[34] (3) Geobarometry based on clinopyroxene and glass compositions gives crystallizing pressures of 5.6–6.4 kbar and 0.6–1.8 kbar corresponding to crystallization depths of 16–18 km and 2–5 km, for the flank and the summit eruption, respectively. These data illustrate that magma chambers are located at different depths beneath the Eyjafjallajökull intrusion.

[35] (4) Plagioclase-melt hygrometry has been employed to constrain water content in the 2010 Eyjafjallajökull eruption. Computed water concentrations using a combination of two hygrometers predict average water concentrations from 0.7 wt % H_2O in the basaltic tephra to 1.8 wt % H_2O obtained in one of the benmorite samples in agreement with data from melt inclusions. Although H_2O clearly influences our geothermobarometry calculations, reasonable estimates of magmatic water concentrations have a limited effect on the results and do not alter our general pressure-temperature conclusions.

[36] **Acknowledgments.** The Icelandic Science Fund and the Carlsberg Foundation supported this research. We would like to thank the whole Eyjafjallajökull team at the Institute of Earth Sciences, University of Iceland, for carrying out sampling often in difficult conditions. We are indebted to Jean-Luc Devidel for help with the microprobe analyses. Journal reviews by Keith Putirka and an anonymous reviewer were very constructive and led to significant improvements in the final version. This is a laboratory of excellence "ClerVolc" contribution number 16.

References

Aulinas, M., D. Gimeno, J. L. Fernandez-Turiel, F. J. Perez-Torrado, A. Rodriguez-Gonzalez, and D. Gasperini (2010), The Plio-Quaternary magmatic feeding system beneath Gran Canaria (Canary Islands, Spain): Constraints from thermobarometric studies, *J. Geol. Soc.*, *167*, 785–801, doi:10.1144/0016-76492009-184.

Beattie, P. (1993), Olivine-melt and orthopyroxene-melt equilbria, *Contrib. Mineral. Petrol.*, *115*, 103–111, doi:10.1007/BF00712982.

Berndt, J., C. Liebske, F. Holtz, M. Freise, M. Nowak, D. Ziegenbein, W. Hurkuck, and J. Koepke, (2002), A combined rapid-quench and H2-membrane setup for internally heated pressure vessels: Description and application for water solubility in basaltic melts, *Am. Mineral.*, *87*, 1717–1726.

Breddam, K. (2002), Kistufell: Primitive melt from the Iceland mantle plume, *J. Petrol.*, *43*, 345–373, doi:10.1093/petrology/43.2.345.

de Zeeuw-van Dalfsen, E., R. Pedersen, F. Sigmundsson, and C. Pagli (2004), Satellite radar interferometry 1993–1999 suggests deep accumulation of magma near the crust-mantle boundary at the Krafla volcanic system, Iceland, *Geophys. Res. Lett.*, *31*, L13611, doi:10.1029/2004GL020059.

de Zeeuw-van Dalfsen, E., H. Rymer, G. Williams-Jones, E. Sturkell, and F. Sigmundsson (2006), Integration of micro-gravity and geodetic data to constrain shallow system mass changes at Krafla Volcano, N. Iceland, *Bull. Volcanol.*, *68*, 420–431, doi:10.1007/s0445-005-0018-5.

Dixon, J. E., E. M. Stolper, and J. R. Holloway (1995), An experimental study of water and carbon dioxide solubilities in mid ocean ridge basaltic liquids.1. Calibration and solubility models, *J. Petrol.*, *36*, 1607–1631.

Droop, G. T. R. (1987), A general equation for estimating Fe^{3+} concentrations in ferromagnesian silicates and oxides from microprobe analyses, using stoichiometric criteria, *Mineral. Mag.*, *51*, 431–435, doi:10.1180/minmag.1987.051.361.10.

Elthon, D. (1989), Pressure of origin of primary mid-ocean ridge basalts, in *Magmatism in the Ocean Basins*, edited by A. D. Saunders and M. J. Norry, *J. Geol. Soc. London*, *42*, 125–136.

Finnerty, A. A., and F. R. Boyd (1978), Pressure-dependent solubility of calcium on forsterite coexisting with diopside and enstatite, *Year Book Carnegie Inst. Washington*, *77*, 713–717.

Furman, T., F. A. Frey, and K.-H. Park (1991), Chemical constraints on the petrogenesis of mildly alkaline lavas from Vestmannaeyjar, Iceland: The Eldfell (1973) and Surtsey (1963–1967) eruptions, *Contrib. Mineral. Petrol.*, *109*, 19–37, doi:10.1007/BF00687198.

Gudmundsson, O. (2003), The dense root of the Iceland crust, *Earth Planet. Sci. Lett.*, *206*, 427–440, doi:10.1016/S0012-821X(02)01110-X.

Gudmundsson, O., B. Brandsdottir, W. Menke, and G. E. Sigvaldason (1994), The crustal magma chamber of the Katla volcano in South Iceland revealed by 2-d seismic undershooting, *Geophys. J. Int.*, *119*, 277–296, doi:10.1111/j.1365-246X.1994.tb00928.x.

Gudmundsson, M. T., R. Pedersen, K. Vogfjörd, B. Thorbjarnardottir, S. Jakobsdottir, and M. Roberts (2010), Eruptions of Eyjafjallajökull Volcano, Iceland, *Eos Trans. AGU*, *91*(21), 190, doi:10.1029/2010EO210002.

Gurenko, A. A., and M. Chaussidon (1995), Enriched and depleted primitive melts included in olivine from Icelandic tholeiites: Origin by continuous melting of a single mantle column, *Geochim. Cosmochim. Acta*, *59*, 2905–2917, doi:10.1016/0016-7037(95)00184-0.

Halldorsson, S. A., N. Oskarsson, K. Gronvold, G. Sigurdsson, G. Sverrisdottir, and S. Steinthorsson (2008), Isotopic-heterogeneity of the Thjorsa lava: Implications for mantle sources and crustal processes within the Eastern Rift Zone, Iceland, *Chem. Geol.*, *255*, 305–316, doi:10.1016/j.chemgeo.2008.06.050.

Hansen, H., and K. Grönvold (2000), Plagioclase ultrapyric basalts in Iceland: The mush of the rift, *J. Volcanol. Geothem. Res.*, *98*, 1–32.

Hansteen, T. H. (1991), Multi-stage evolution of the picritic Maelifell Rocks, SW Iceland: Constraints from mineralogy and inclusions of glass

and fluid in olivine, *Contrib. Mineral. Petrol.*, *109*, 225–239, doi:10.1007/BF00306481.

Hards, V. L., P. D. Kempton, R. N. Thompson, and P. B. Greenwood (2000), The magmatic evolution of the Snæfell volcanic centre; an example of volcanism during incipient rifting in Iceland, *J. Volcanol. Geotherm. Res.*, *99*, 97–121, doi:10.1016/S0377-0273(00)00160-8.

Herzberg, C. (2004), Partial crystallization of mid-ocean ridge basalts in the crust and mantle, *J. Petrol.*, *45*, 2389–2405, doi:10.1093/petrology/egh040.

Housh, T. B., and J. F. Luhr (1991), Plagioclase-melt equilibria in hydrous systems, *Am. Mineral.*, *76*, 477–492.

Irvine, N. T., and W. R. A. Baragar (1971), A guide to the chemical classification of the common volcanic rocks, *Can. J. Earth Sci.*, *8*, 523–548, doi:10.1139/e71-055.

Kelley, D. F., and M. Barton (2008), Pressures of crystallization of Icelandic magmas, *J. Petrol.*, *49*, 465–492, doi:10.1093/petrology/egm089.

Kent, A. J. R. (2008), Melt inclusions in basaltic and related volcanic rocks, *Rev. Mineral. Geochem.*, *69*, 273–331, doi:10.2138/rmg.2008.69.8.

Key, J., R. S. White, H. Soosalu, and S. S. Jakobsdóttir (2011), Multiple melt injection along a spreading segment at Askja, Iceland, *Geophys. Res. Lett.*, *38*, L05301, doi:10.1029/2010GL046264.

Klügel, A., T. H. Hansteen, and K. Galipp (2005), Magma storage and underplating beneath Cumbre Vieja Volcano, La Palma (Canary Islands), *Earth Planet. Sci. Lett.*, *236*, 211–226, doi:10.1016/j.epsl.2005.04.006.

Kudo, A. M., and D. F. Weill (1970), An igneous plagioclase thermometer, *Contrib. Mineral. Petrol.*, *25*, 52–65, doi:10.1007/BF00383062.

Kushiro, I. (1969), The system forsterite-diopside-silica with and without water at high pressures, *Am. J. Sci.*, *267-A*, 269–294.

Lange, R. A., H. M. Frey, and J. Hector (2009), A thermodynamic model for the plagioclase-liquid hygrometer/thermometer, *Am. Mineral.*, *94*, 494–506, doi:10.2138/am.2009.3011.

Le Maitre, R. W., A. Streckeisen, B. Zanettin, M. J. Le Bas, B. Bonin, and P. Bateman (Eds.) (2005), *Igneous Rocks: A Classification and Glossary of Terms: Recommendations of the International Union of Geological Sciences Subcommission on the Systematics of Igneous Rocks*, 2nd ed., 256 pp., Cambridge Univ. Press, Cambridge, U. K.

Lee, C.-T. A., P. Luffi, T. Plank, H. Dalton, and W. P. Leeman (2009), Constraints on the depths and temperatures of basaltic magma generation on Earth and other terrestrial planets using new thermobarometers for mafic magmas, *Earth Planet. Sci. Lett.*, *279*, 20–33, doi:10.1016/j.epsl.2008.12.020.

Lindsley, D. H. (1983), Pyroxene thermometry, *Am. Mineral.*, *68*, 477–493.

Lowenstern, J. B. (1995), Applications of silicate melt inclusions to the study of magmatic volatiles, in *Magmas, Fluid and Ore Deposits*, *Short Course Ser.*, vol. 23, edited by J. F. H. Thompson, pp. 71–99, Mineral. Assoc. of Can., Victoria, B. C.

Maclennan, J., D. McKenzie, K. Grönvold, and L. Slater (2001), Crustal accretion under northern Iceland, *Earth Planet. Sci. Lett.*, *191*, 295–310, doi:10.1016/S0012-821X(01)00420-4.

Mathez, E. A. (1973), Refinement of the Kudo-Weill plagioclase thermometer and its applications to basaltic rocks, *Contrib. Mineral. Petrol.*, *41*, 61–72, doi:10.1007/BF00377654.

Menke, W. (1999), Crustal isostasy indicates anomalous densities beneath Iceland, *Geophys. Res. Lett.*, *26*, 1215–1218, doi:10.1029/1999GL900202.

Mollo, S., P. Del Gaudio, G. Ventura, G. Iezzi, and P. Scarlato (2010), Dependence of clinopyroxene composition on cooling rate in basaltic magmas: Implications for thermobarometry, *Lithos*, *118*, 302–312, doi:10.1016/j.lithos.2010.05.006.

Mollo, S., K. Putirka, G. Iezzi, P. Del Gaudio, and P. Scarlato (2011), Plagioclase-melt (dis)equilibrium due to cooling dynamics: Implications for thermometry, barometry and hygrometry, *Lithos*, *125*, 221–235, doi:10.1016/j.lithos.2011.02.008.

Mordick, B. E., and A. F. Glazner (2006), Clinopyroxene thermobarometry of basalts from the Coso and Big Pine volcanic fields, California, *Contrib. Mineral. Petrol.*, *152*, 111–124, doi:10.1007/s00410-006-0097-0.

Morimoto, N. (1989), Nomenclature of pyroxenes, *Can. Mineral.*, *27*, 143–156.

Moune, S., O. Sigmarsson, T. Thordarson, P. Schiano, and J. K. Keiding (2012), Melt inclusion constraints on the magma source of Eyjafjallajökull 2010 flank eruption, *J. Geophys. Res.*, *117*, B00C07, doi:10.1029/2011JB008718.

Nimis, P. (1995), A clinopyroxene geobarometer for basaltic systems based on crystal-structure modeling, *Contrib. Mineral. Petrol.*, *121*, 115–125, doi:10.1007/s004100050093.

Nimis, P., and P. Ulmer (1998), Clinopyroxene geobarometry of magmatic rocks, Part 1: An expanded structural geobarometer for anhydrous and hydrous, basic and ultrabasic systems, *Contrib. Mineral. Petrol.*, *133*, 122–135, doi:10.1007/s004100050442.

O'Hara, M. J. (1968), Are ocean floor basalts primary magma?, *Nature*, *220*, 683–686, doi:10.1038/220683a0.

Óladóttir, B. A., O. Sigmarsson, G. Larsen, and T. Thordarson (2008), Katla volcano, Iceland: Magma composition, dynamics and eruption frequency as recorded by Holocene tephra layers, *Bull. Volcanol.*, *70*, 475–493, doi:10.1007/s00445-007-0150-5.

Panjasawatwong, Y., L. V. Danyushevsky, A. J. Crawford, and K. L. Harris (1995), An experimental study of the effects of melt composition on plagioclase-melt equilibria at 5 and 10 kbar: Implications for the origin of magmatic high-An plagioclase, *Contrib. Mineral. Petrol.*, *118*, 420–432, doi:10.1007/s004100050024.

Pedersen, R., and F. Sigmundsson (2004), InSAR based sill model links spatially offset areas of deformation and seismicity for the 1994 unrest episode at Eyjafjallajökull volcano, Iceland, *Geophys. Res. Lett.*, *31*, L14610, doi:10.1029/2004GL020368.

Pedersen, R., and F. Sigmundsson (2006), Temporal development of the 1999 intrusive episode in the Eyjafjallajökull volcano, Iceland, derived from InSAR images, *Bull. Volcanol.*, *68*, 377–393, doi:10.1007/s00445-005-0020-y.

Powell, M., and R. Powell (1974), An olivine-clinopyroxene geothermometer, *Contrib. Mineral. Petrol.*, *48*, 249–263, doi:10.1007/BF00951333.

Putirka, K. D. (2005), Igneous thermometers and barometers based on plagioclase plus liquid equilibria: Tests of some existing models and new calibrations, *Am. Mineral.*, *90*, 336–346, doi:10.2138/am.2005.1449.

Putirka, K. D. (2008), Thermometers and barometers for volcanic systems, *Rev. Mineral. Geochem.*, *69*, 61–120, doi:10.2138/rmg.2008.69.3.

Putirka, K., M. Johnson, R. Kinzler, J. Longhi, and D. Walker (1996), Thermobarometry of mafic igneous rocks based on clinopyroxene-liquid equilibria, 0–30 kbar, *Contrib. Mineral. Petrol.*, *123*, 92–108, doi:10.1007/s004100050145.

Roedder, E. (1984), *Fluid Inclusions*, *Rev. Mineral.*, vol. 12, 644 pp., Mineral. Soc. of Am., Washington, D. C.

Roeder, P. L., and R. F. Emslie (1970), Olivine-liquid equilibrium, *Contrib. Mineral. Petrol.*, *29*, 275–289, doi:10.1007/BF00371276.

Schiellerup, H. (1995), Generation and equilibration of olivine tholeiites in the Northern rift-zone of Iceland: A petrogenetic study of the Blafjall table mountain, *J. Volcanol. Geotherm. Res.*, *65*, 161–179, doi:10.1016/0377-0273(94)00116-X.

Schopka, H. H., M. T. Gudmundsson, and H. Tuffen (2006), The formation of Helgafell, southwest Iceland a monogenetic subglacial hyaloclastite ridge: Sedimentology, volcano-ice interaction hydrology and, *J. Volcanol. Geotherm. Res.*, *152*, 359–377, doi:10.1016/j.jvolgeores.2005.11.010.

Shishkina, T. A., R. E. Botcharnikov, F. Holtz, R. R. Almeev, and M. V. Portnyagin (2010), Solubility of H_2O- and CO_2-bearing fluids in tholeiitic basalts at pressures up to 500 MPa, *Chem. Geol.*, *277*, 115–125, doi:10.1016/j.chemgeo.2010.07.014.

Sigmarsson, O., M. Condomines, and S. Fourcade (1992), A detailed Th, Sr and O isotope study of Hekla: Differentiation processes in an Icelandic Volcano, *Contrib. Mineral. Petrol.*, *112*, 20–34, doi:10.1007/BF00310953.

Sigmarsson, O., T. Thordarson, and S. P. Jakobsson (2009), Segregations in Surtsey lavas (Iceland) reveal extreme magma differentiation during late stage flow emplacement, in *Studies in Volcanology: The Legacy of George Walker*, *Spec. Publ. IAVCEI*, vol. 2, edited by T. Thordason et al., pp. 85–104, Geol. Soc. London, London.

Sigmarsson, O., I. Vlastelic, R. Andreasen, I. Bindeman, J.-L. Devidal, S. Moune, J. K. Keiding, G. Larsen, A. Höskuldsson, and T. Thordarson (2011), Remobilization of silicic intrusion by mafic magmas during the 2010 Eyjafjallajökull eruption, *Solid Earth*, *2*, 271–281, doi:10.5194/se-2-271-2011.

Sigmundsson, F., et al. (2010), Intrusion triggering of the 2010 Eyjafjallajökull explosive eruption, *Nature*, *468*, 426–430, doi:10.1038/nature09558.

Sigurdsson, H., and R. S. J. Sparks (1981), Petrology of rhyolitic and mixed magma ejecta from the 1875 eruption of Askja, Iceland, *J. Petrol.*, *22*, 41–81.

Sisson, T. W., and T. L. Grove (1993), Temperatures and H_2O contents of low-MgO high-alumina basalts, *Contrib. Mineral. Petrol.*, *113*, 167–184, doi:10.1007/BF00283226.

Slater, L., D. McKenzie, K. Grönvold, and N. Shimizu (2001), Melt generation and movement beneath Theistareykir, NE Iceland, *J. Petrol.*, *42*, 321–354, doi:10.1093/petrology/42.2.321.

Soosalu, H., and P. Einarsson (2004), Seismic constraints on magma chambers at Hekla and Torfajokull volcanoes, Iceland, *Bull. Volcanol.*, *66*, 276–286, doi:10.1007/s00445-003-0310-1.

Soosalu, H., K. Jónsdóttir, and P. Einarsson (2006), Seismicity crisis at the Katla volcano, Iceland: Signs of a cryptodome?, *J. Volcanol. Geotherm. Res.*, *153*, 177–186, doi:10.1016/j.jvolgeores.2005.10.013.

Soosalu, H., J. Key, R. S. White, C. Knox, P. Einarsson, and S. S. Jakobsdóttir (2010), Lower-crustal earthquakes caused by magma movement beneath

Askja volcano on the north Iceland rift, *Bull. Volcanol.*, *72*, 55–62, doi:10.1007/s00445-009-0297-3.

Stroncik, N. A., A. Klügel, and T. H. Hansteen (2009), The magmatic plumbing system beneath El Hierro (Canary Islands): Constraints from phenocrysts and naturally quenched basaltic glasses in submarine rocks, *Contrib. Mineral. Petrol.*, *157*, 593–607, doi:10.1007/s00410-008-0354-5.

Sturkell, E., F. Sigmundsson, and P. Einarsson (2003), Recent unrest and magma movements at Eyjafjallajökull and Katla volcanoes, Iceland, *J. Geophys. Res.*, *108*(B8), 2369, doi:10.1029/2001JB000917.

Sturkell, E., P. Einarsson, F. Sigmundsson, H. Geirsson, H. Olafsson, R. Pedersen, E. de Zeeuw-van Dalfsen, A. T. Linde, S. I. Sacks, and R. Stefansson (2006), Volcano, geodesy and magma dynamics in Iceland, *J. Volcanol. Geotherm. Res.*, *150*, 14–34, doi:10.1016/j.jvolgeores.2005.07.010.

Thorarinsson, S. B., and C. Tegner (2009), Magma chamber processes in central volcanic systems of Iceland: Constraints from layered gabbro of the Austurhorn intrusive complex, *Contrib. Mineral. Petrol.*, *158*, 223–244, doi:10.1007/s00410-009-0379-4.

Thordarson, T., C. Hayward, S. Moune, M. E. Hartley, O. Sigmarsson, A. Höskuldsson, M. T. Guðmundsson, and F. Sigmundsson (2011), The 20 March–12 April 2010 Fimmvörðuháls eruption, Eyjafjallajökull volcano, Iceland: Volatile contents and magma degassing, paper EGU2011-12147 presented at EGU General Assembly, Vienna.

Thy, P. (1991), High and low pressure phase equilibria of a mildly alkalic lava from the 1965 Surtsey eruption: Experimental results, *Lithos*, *26*, 223–243, doi:10.1016/0024-4937(91)90030-O.

Villiger, S., O. Müntener, and P. Ulmer (2007), Crystallization pressures of mid-ocean ridge basalts derived from major element variations of glasses from equilibrium and fractional crystallization experiments, *J. Geophys. Res.*, *112*, B01202, doi:10.1029/2006JB004342.

Wager, L. R., and G. M. Brown (1968), *Layered Igneous Rocks*, 588 pp., Oliver and Boyd, Edinburgh, U. K.

White, R. S., J. Drew, H. R. Martens, J. Key, H. Soosalu, and S. S. Jakobsdóttir (2011), Dynamics of dyke intrusion in the mid-crust of Iceland, *Earth Planet. Sci. Lett.*, *304*, 300–312, doi:10.1016/j.epsl.2011.02.038.

Yang, H. J., R. J. Kinzler, and T. L. Grove (1996), Experiments and models of anhydrous, basaltic olivine-plagioclase-augite saturated melts from 0.001 to 10 kbar, *Contrib. Mineral. Petrol.*, *124*, 1–18, doi:10.1007/s004100050169.

J. K. Keiding, GFZ German Research Centre for Geosciences, Telegrafenberg, D-14473 Potsdam, Germany. (jakob@gfz-potsdam.de)

O. Sigmarsson, Laboratoire Magmas et Volcans, CNRS-Université Blaise Pascal, F-63038 Clermont-Ferrand, France.